Applied Catalysis B: Environmental 140–141 (2013) 125–132

Contents lists available at SciVerse ScienceDirect

Applied Catalysis B: Environmental

journal homepage: www.elsevier.com/locate/apcatb

Co-B catalyst supported over mesoporous silica for hydrogen production by catalytic hydrolysis of Ammonia Borane: A study on influence of pore structure

N. Patel[a,*], R. Fernandes[a], S. Gupta[b], R. Edla[a], D.C. Kothari[b], A. Miotello[a]

[a] Dipartimento di Fisica, Università degli Studi di Trento, I-38123 Povo (Trento), Italy
[b] Department of Physics, University of Mumbai, Vidyanagari, Santacruz (E), Mumbai 400098, India

ARTICLE INFO

Article history:
Received 20 February 2013
Received in revised form 19 March 2013
Accepted 27 March 2013
Available online 2 April 2013

Keywords:
Cobalt Boride
Mesoporous silica
Ammonia Borane
Hydrogen generation
Nanoparticles

ABSTRACT

Three kinds of mesoporous silica (MCM-41, FSM-16 and SBA-15) of different pore size and texture were synthesized by templating method. Co-B nanoparticle catalysts were supported over these mesoporous silica by impregnation–reduction method in order to study the effect of support pore structure on the catalytic properties in H_2 production by hydrolysis of Ammonia Borane (AB). TEM and N_2 adsorption–desorption isotherm results clearly revealed that size, dispersion degree, and location of Co-B particle is affected by the pore texturing of the support. It also showed that the catalyst particle acquires directly the size of the support pores only for SBA-15 whereas there is no correlation of the particle size and pore size for MCM-41 and FSM-16. Co-B supported over SBA-15 silica was found to be the most active catalyst as inferred from the observed hydrogen generation rates in the hydrolysis reaction compared to that produced by MCM-41 and FSM-16 supported catalyst. Higher activity for SBA-15 support is mainly attributed to the geometrical confinement of Co-B particles within the pores which creates smaller Co-B particles (6 nm) with uniform size distribution and higher degree of dispersion as compared to MCM-41 and FSM-16 support where the Co-B particles lie on the external surface with broad size distribution. Open and interconnected pores of SBA-15 can also provide easy passage for reactant and product during the course of reaction. The Co-B particles supported in the interconnected pores of SBA-15 produce lower effective activation energy barrier related to the hydrolysis process of AB than that established with MCM-41 and FSM-16 supported catalyst. Most importantly, the thicker pore walls of SBA-15 assist in avoiding the agglomeration of Co-B particles and even provide high stability at elevated temperatures (873 K) at which unsupported Co-B catalyst gets completely destroyed.

1. Introduction

Hydrogen has been identified as a most efficient energy carrier which when used in fuel cell produces almost zero emission of greenhouse gases. However, the current production of H_2 is mostly based on steam reforming of natural gas where the final products contain greenhouse gases (CO_2 and CO). Thus, it is necessary to implement cleaner routes to produce H_2 using least amount of energy to make the hydrogen energy cycle environmentally green. Hydrolysis of chemical hydrides is the best path to produce pure H_2 without using any energy at room temperature even if regeneration of spent hydrides would require energy that could be taken from renewable energy sources. With high gravimetric storage (19.6 wt%) capacity, Ammonia Borane (NH_3BH_3, AB) is the most attractive source for the supply of pure H_2 via hydrolysis reaction for portable and on-board applications with fuel cell at room temperature [1,2]. However, catalyst is the key material to control the H_2 generation rate during the hydrolysis reaction.

Generally, precious metals have been traditionally used in the past as the catalyst to accelerate the H_2 production rate. But the cost and availability of these materials prompted researchers to find cheaper alternatives [3–6]. Transition metals such as Co and Ni, when fabricated on nano scale with high surface area, can exhibit catalytic performance comparable to that of noble metals. Recently, we showed that Co nanoparticles (NPs) based catalyst produced by pulsed laser deposition is able to generate H_2 with the rate similar to Pt and much higher than Pd catalyst by the hydrolysis of chemical hydrides [7,8]. Among the low cost materials, Cobalt Boride (Co-B) showed an exceptional catalytic activity mainly owing to its unique properties with high concentration of coordinative unsaturated sites, and its chemical stability [9,10]. In addition, Co-B can be produced by simple chemical reduction of cobalt salt. However, due to the exothermic nature of the reduction reaction and ferromagnetic nature of the material, the produced Co-B NPs agglomerate

* Corresponding author. Tel.: +39 0461 282012.
E-mail addresses: patel@science.unitn.it, nainesh11@gmail.com (N. Patel).

0926-3373/$ – see front matter © 2013 Elsevier B.V. All rights reserved.
http://dx.doi.org/10.1016/j.apcatb.2013.03.046

to reduce the effective surface area which in turn hampers the catalytic activity considerably. Several routes were adopted in the past to avoid the agglomeration such as by doping with transition metals [11–13], by using organic templates [14] or by supporting the catalyst on high surface area materials such as rough carbon [15,16]. However, the preparation of catalyst NPs of desired size, which allows tuning of catalytic activity, still remains a challenge. Thus, it is of paramount importance in developing a system that can provide a degree of freedom to control the size of the catalyst NPs during preparation as well as to maintain this size during the catalytic reaction and also at elevated temperatures. Thus, due to all these reasons, catalyst particles supported over porous materials such as alumina, silica, carbon, and zeolites seems to be a better option to deliver sustainable solution with improved catalytic activity.

In such supported catalyst, the NPs acquire the size of pores which can be easily tuned using various templates and synthetic pathways. When confined into the pore channels, catalyst NPs attain high resistance against agglomeration as they are isolated from each other in the solid matrix. Microporous materials (pores size < 2 nm) such as zeolite can trap and produce smaller NPs but the diffusion of reactant in the small pores to the internal catalytically active sites is restricted [17]. Thus, mesoporous silica materials with highly ordered structure are the most appropriate candidate as the support material for the catalyst NPs. Mesoporous silica of various type (SBA-15, FSM-16, MCM-41, HMS, etc.) possess high specific surface area, large pore volume, highly ordered pore structure, narrow size distribution and most importantly the pore size can be tuned from 2 to 50 nm with minimum effort [18–20]. Their large and interconnected channels allow easy passage for the reactant and product and also offer shape related selectivity. The pore walls of mesoporous silica hold very high strength at elevated temperature and in corrosive environment to withstand against the disintegration of the pore structure. Several kinds of metal NPs, mainly precious metals such as Pd [17], Pt [21], Ru [22], Au [23], and Ag [24] were supported in the pore channels of mesoporous silica in order to acquire desired size and minimize the usage of these metals. Ni-B [25] and Co-B [26] catalyst supported over mesoporous silica have been effectively used for the hydrogenation reaction with enhanced activity and selectivity. These supported metal NPs not only provide high catalytic activity and selectivity but also show high resistance and stability for long term usage.

The present work is focused on the synthesis of Co-B NPs within the pores of mesoporous silica in order to achieve both control and maintain uniform particle size having high degree of dispersion and resistance against deactivation due to sintering at elevated temperatures. For this purpose, Co-B catalyst NPs were supported over three types of mesoporous silica (MCM-41, FSM-16, SBA-15) of different pore size and texture by impregnation–reduction method. Catalytic performance of these supported NPs was tested for the H_2 production by hydrolysis of AB. Based on several characterization results, the connection between pore structures of the mesoporous silica and the size, location, and dispersion of Co-B NPs was established which are correlated to the obtained catalytic variation in the hydrolysis of AB.

2. Experimental methods

Three different types of Mesoporous Silica Particles (MSP) were synthesized to support the Co-B NPs catalyst. All the chemicals used for the synthesis were acquired from Sigma Aldrich. The synthesis procedure adopted is as follows:

MCM-41: This type of mesoporous silica particles was synthesized, following the procedure described in Lai et al. [27], by using *n*-cetyltrimethylammonium bromide (CTAB) as the surfactant template to assemble mesopores on the surface. CTAB (0.25 g) was first dissolved in 120 ml of deionized water and stirred for 30 min. NaOH (2 M, 0.875 ml), as a catalyst, was added to the above mixture, followed by adjusting the temperature at 353 K. Dropwise addition of tetraethylorthosilicate (TEOS, 99.999%) (1.25 ml) was carried out to the surfactant solution and resulting mixture was stirred at 353 K for 2 h to obtain white silica precipitate. The solid powder obtained by centrifuging was washed thoroughly with distilled water and dried in vacuum condition at ambient temperature. After drying, silica powder (0.7 g) was refluxed in solution of 70 ml of methanol and 3.5 ml of HCl (35%) for 24 h in order to remove surfactant template (CTAB) over the surface. The white powder was separated by centrifuging the solution and later washed with distilled water and methanol followed by drying in vacuum. The obtained powder was treated at 398 K for 2 h to remove the OH^- group from the pore surface.

FSM-16: Kanemite ($NaHSi_2O_5$) and CTAB were used as precursor and template, respectively, to synthesize FSM-16 type MSP following the method described in [28]. To synthesize kanemite, sodium hydroxide of 100 ml (0.528 M) was added to 50 g of sodium silicate solution ($SiO_2/Na_2O = 2.21$) to adjust $SiO_2/Na_2O = 2$. The mixture was stirred for 3 h at ambient temperatures. The excess water was removed by drying the solution at 393 K for 15 h. After crushing, the dried sodium silicate powder was calcinated at 973 K for 6 h in air to obtain white kanemite foam. Crushed kanemite powder (2 g) was dispersed in 20 ml of distilled water and stirred for 3 h. The resulting suspension was filtered out to obtain wet kanemite paste. This paste was mixed into 32 ml of CTAB (0.125 M) solution and then stirred for 3 h at 343 K. The pH of the dispersion was adjusted to 8.5 by adding HCl solution (2 M). The resulting mixture was stirred for another 3 h at 343 K. After cooling, filtered solid powder was washed with distilled water and then dried in air at ambient temperature. The as-synthesized silica powder was calcinated at 873 K for 6 h to remove the surfactant from the silica material to obtain FSM-16 MSP.

SBA-15: Pluronic (P123) was used as the surfactant template to fabricate SBA type MSP. The synthesis was carried out without hydrothermal conditions using the procedure described in Brahmkhatri et al. [29]. P123 (4 g) was first dissolved in 150 ml of HCl solution (2 M) under constant stirring at 308 K for 2 h. Later TEOS (8.5 g) was added to the above mixture and stirred for 20 h at 308 K. The resulting solution mixture was aged at 353 K for 48 h. The solid powder was separated by filtration and followed by washing with distilled water and ethanol. After drying at room temperature, the white powder was calcinated at 773 K for 6 h to burnout template molecules from the silica material.

Non-Porous Silica (NPS) particles were also prepared by Stober method [30] by hydrolysis and condensation of TEOS in ethanol, and in the presence of ammonia (NH_3) as catalyst. The molar ratio of TEOS:NH_3:H_2O:ethanol was kept about 1:1:10:30.

The Co-B catalyst was loaded on NPS particles and on three different types of MSP (MCM-41, SBA-15 and FSM-16) by impregnation–reduction method. 300 mg of all types of silica particles were immersed in the 4.5 ml of aqueous cobalt chloride solution (0.5 M). To have better particle dispersion the mixture was ultra-sonicated for 10 min and later left undisturbed for 24 h. After impregnation the samples were filtered to remove the excess $CoCl_2$ solution and dried in vacuum condition. The dried mixture was reduced by addition of 4.5 ml of aqueous $NaBH_4$ solution (1 M) and later stirred until the bubbles generation was ceased. The gray powder formed during the reaction was separated from the solution by sedimentation and filtration and later washed several times with distilled water and ethanol. In the end the catalyst was dried in vacuum under ambient condition. Co-B powder was also synthesized for comparison by reducing cobalt chloride solution.

Structural characterization of the silica supports in small-angle and wide-angle was performed by conventional X-ray diffraction

(XRD) using the Cu K_α radiation ($\lambda = 1.5414$ Å) in Bragg–Brentano (θ–2θ) configuration. The BET surface area of the silica particles and Co-B supported over silica was determined by nitrogen absorption at 77 K using Quantachrome instrument (QuadraSorb 5.04) after degassing at 473 K for 2 h. Pore size, pore wall thickness, Co-B particle size, and pore structure were examined using a transmission electron microscope (TEM, JEOL-JEM 2100F and energy of 200 keV). A suspension of the particles in distilled water was sonicated for 15 min and a drop was placed onto a copper grid which was examined in TEM after solvent drying. The amount of Co-B loading in mesoporous silica was established by energy-dispersive spectroscopy analysis (EDS, INCA PentaFET-x3) equipped with scanning electron microscope (SEM-FEG, JSM 7001F, JEOL).

For catalytic activity measurements, a solution of Ammonia Borane (0.025 ± 0.001 M) (Sigma Aldrich) was prepared. Gas volumetric method was used to measure the hydrogen volume generated by hydrolysis reaction. Detailed description of the measurement apparatus can be found elsewhere [31]. In the present experiment, 150 ml of the above AB solution was maintained at the desired temperature and then catalyst powder was added to this solution. H_2 production rate was calculated by measuring the weight of the water displaced which can be easily converted into cumulative hydrogen production yield (%) and plotted against the reaction time. To determine the activation energy involved in the catalytic hydrolysis, H_2 generation rate was measured at different solution temperatures. In order to test the stability of the Co-B catalyst supported mesoporous silica at high temperature, all the catalyst powders were calcinated at 3 different temperatures of 673 K, 773 K, and 873 K for 2 h in Ar atmosphere. The effect on the catalytic activity in these heat-treated powders was studied through catalytic hydrolysis of AB.

3. Results and discussion

Small-angle XRD (SAXRD) patterns of NPS, MCM-41, FSM-16 and SBA-15 silica particles are reported in Fig. 1. No evidence of any peak in the pattern of NPS particles clearly indicates the absence of porosity. While a single peak is observed at 2θ values of 2.23° and 2.61° for MCM-41 and FSM-16 silica, respectively, which is indexed as (1 0 0) reflection. On the other hand, SBA-15 type silica prepared by nonionic block copolymer surfactant displays three well-resolved diffraction peaks at 1.05°, 1.68°, and 1.92° which can be indexed as (1 0 0), (1 1 0) and (2 0 0) reflections associated with *p6mm* hexagonal symmetry [32]. All these peaks in the mesoporous

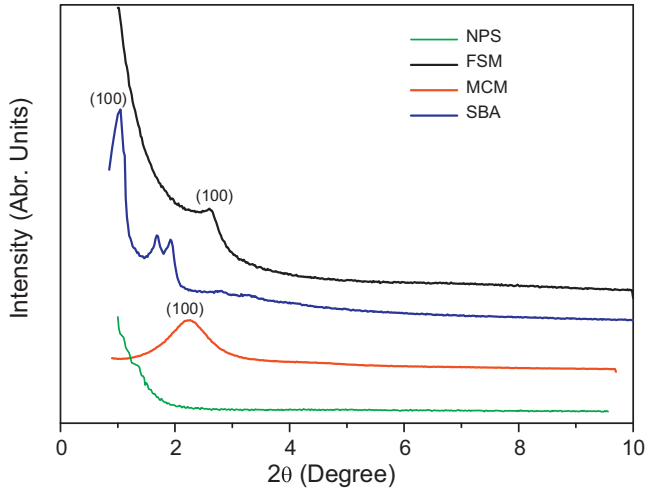

Fig. 1. Small-angle XRD pattern of NPS, MCM-41, FSM-16 and SBA-15 type silica materials.

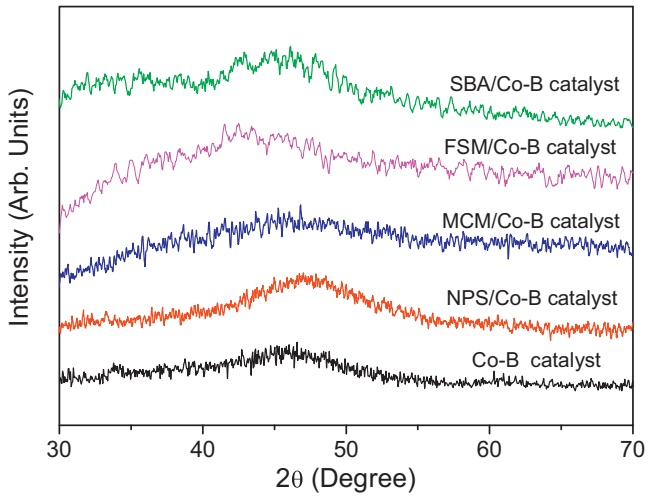

Fig. 2. Wide-angle XRD pattern of unsupported Co-B powder and that supported on NPS, MCM-41, FSM-16, and SBA-15 type silica materials.

silica are assigned to the regular array of hexagonal pore structure. The presence of higher order reflections demonstrate that SBA-15 silica acquire highly ordered hexagonal array of pores with uniform pore size as compared to MCM-41 and FSM-16 silica, which is also confirmed by TEM results (see below). The intensity of the characteristic reflection peaks decreases in XRD patterns (figure not shown) after Co-B loading. Thus catalyst introduction probably plugs the pores and disturbs the local symmetry of the channel packing. In addition, X-ray mass absorption coefficient of cobalt is much higher than those of silicon and oxygen constituting the SiO_2 structure [33].

XRD pattern in wide-range for unsupported Co-B catalyst and supported over NPS, MCM-41, FSM-16 and SBA-15 silica particles are reported in Fig. 2. The broad peak at around $2\theta = 45°$ assigned to the amorphous state of Co-B alloy is observed for unsupported and supported over NPS. On the contrary, no peak of Co-B is observed for the catalyst supported over all the three mesoporous silica particles, thus indicating that the catalyst species were highly dispersed in the pores of the support material. The diffraction pattern indicates short-range order and long-range disorder of Co-B alloy and both features are expected to enhance the catalytic activity [9].

XPS analysis of the unsupported Co-B powder conducted in our previous work [13] showed an electronic transfer from alloying B to vacant d-orbital of metallic Co. The Co/B atomic ratio was about 1.5. No major difference was observed in elemental peak position and Co/B atomic ratio from present XPS spectra of Co-B supported on mesoporous silica. Important aspects of this result is that electron-enriched Co sites are most favorable to the catalytic hydrolysis process of AB because the excess electrons contribute to the hydrolysis reaction by providing the charges required by the hydrogen atom to get detached from the catalyst surface [8], thus establishing optimum interaction with the reactant and product molecules.

Nitrogen adsorption–desorption isotherms of all the three mesoporous silica supports (MCM-41, FSM-16 and SBA-15) before and after Co-B loading are presented in Fig. 3. The inset of these figures shows the pore size distribution calculated using BJH method. The physicochemical parameters such as BET surface area, average pore diameter, and pore volume obtained from the isotherm are summarized in Table 1. All these mesoporous silica showed Type IV adsorption–desorption isotherm according to the IUPAC classification [34]. This kind of shape is typical characteristic of mesoporous material with tubular pores [35]. The Type IV isotherm generally

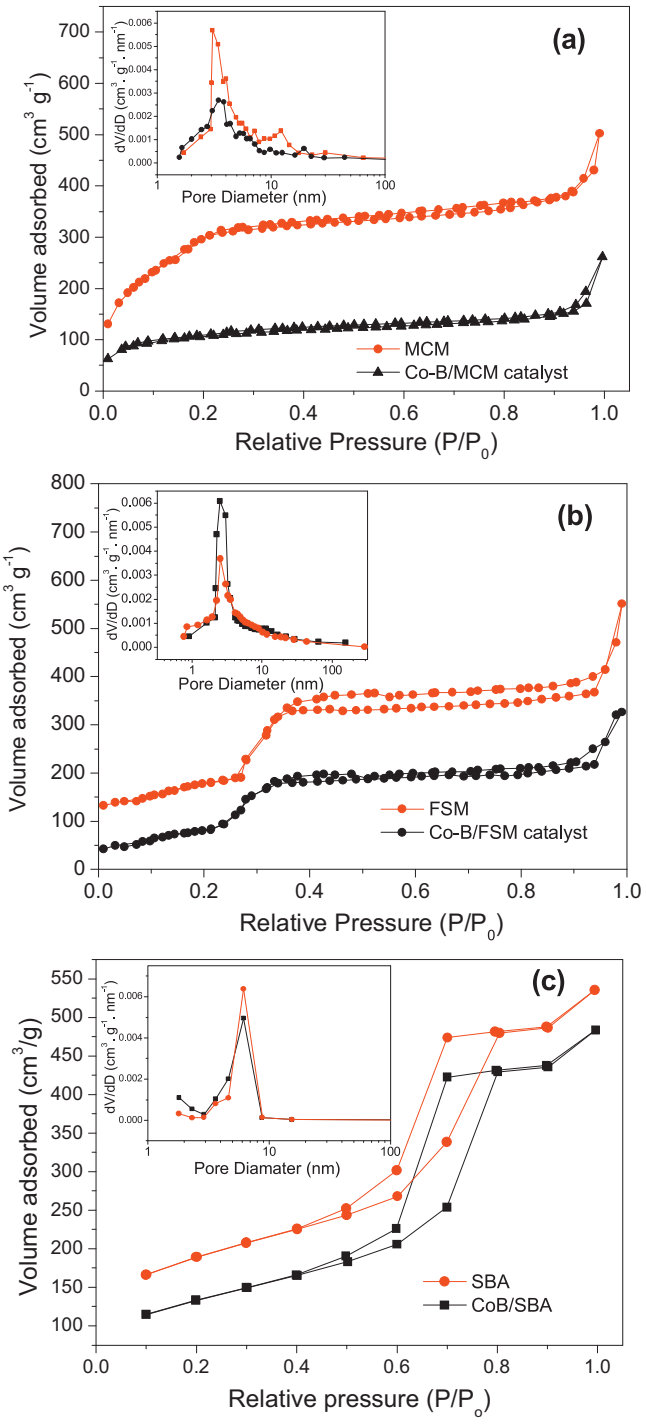

Fig. 3. Nitrogen adsorption–desorption isotherms of (a) MCM-41, (b) FSM-16 and (c) SBA-15 type mesoporous silica supports with and without Co-B catalyst loading. Inset of the figures shows the pore size distribution curves of the corresponding mesoporous silica supports.

signals three regions. Initially at low P/P_0, the flat region is related to the monolayer formation on the silica outer surface and on the pore walls. As the P/P_0 increases, due to the spontaneous filling of the mesopores by the capillary condensation a certain step or inflection is observed in the volume of gas adsorbed. Later volume increases gradually with the P/P_0 and is mainly attributed to the multilayer adsorption on the outer surface of the particle. Finally, significant rise in N_2 adsorption at $P/P_0 > 0.9$ is caused by the filling of macropores formed by the gaps between the silica particles. The

Table 1
Physico-chemical properties of non-porous and three different mesoporous silica supports (MCM-41, FSM-16, and SBA-15) with and without Co-B catalyst loading.

Samples	BET surface area (m^2/g)	Average pore diameter (nm)	Pore volume (cm^3/g)
Co-B powder	20	–	–
NPS	31.5	–	–
Co-B/NPS	11	–	–
MCM-41	970	3.4	0.86
Co-B/MCM-41	335	3.1	0.35
FSM-16	958	2.52	0.85
Co-B/FSM-16	630	2.50	0.62
SBA-15	627	6.15	0.83
Co-B/SBA-15	455	6.14	0.64

sharpness of the inflection indicates the uniformity of the mesopores size distribution. Thus, Fig. 3 shows that the mesopores of SBA-15 and FSM-16 attain narrow size distribution as compared to MCM-41 silica. The inflection region is extended in P/P_0 range from 0.05 to 0.30 (Fig. 3a) for MCM-41 silica with the pore size distribution in the range of 2–8 nm (inset of Fig. 3a). Another important characteristic of the mesopores can be obtained from the shape of adsorption–desorption hysteresis loop of the isotherm which are correlated with the texture of the adsorbent. SBA-15 silica showed H1 type hysteresis loop corresponding to ordered porous material with cylindrical pores open at both ends and interconnected pore structure [36]. H4 type hysteresis loop is demonstrated by the FSM-16 type silica indicating the mixture of microporous (pore size less than 2 nm) and mesoporous structure [34]. On the contrary, distinct hysteresis loop is not observed in case of MCM-41 type silica. Though pore volume of all the three mesoporous silica is nearly same, the average pore size decreases in order of SBA-15 (6.1 nm) > MCM-41 (3.4 nm) > FSM-16 (2.5 nm). Pore wall thickness (Table 2) was calculated by subtracting the pore diameter from the spacing between the regular array of pores (a_o) (obtained from the formula $\{a_o = 1.154 \times d_{100}\}$, where d_{100} is estimated from the first peak in SAXRD (Fig. 1)). The wall thickness of SBA-15 is two times thicker than that of MCM-41 and FSM-16, thus showing the strength and the robustness of pore structure of SBA-15 type silica. The BET surface area of SBA-15 is lower than that of MCM-41 and FSM-16 type due to larger pore size and pore wall thickness. Incorporation of Co-B catalyst to SBA-15 silica did not influence the shape of the isotherm. In contrast, incorporation of Co-B to MCM-41 silica caused significant variation in the lineshape of the isotherms, where inflection characteristic completely disappeared. While in case of FSM-16, the inflection is still present after loading Co-B but the sharpness of the step is decreased along with fading of hysteresis loop. The average pore diameter remains more or less intact for all the three mesoporous materials even after incorporation of Co-B (Table 1). However, the pore volume and BET surface area decreases on Co-B loading with more prominent effect in MCM-41 as compared to SBA-15 and FSM-16. The above results clearly suggests that Co-B particles are located inside the pores of SBA-15 silica by keeping the pore structure intact while for MCM-41 catalyst particles either completely fill the pores or lie outside on the face of pores thus making the pores inaccessible to nitrogen. In case of FSM-16,

Table 2
Pore wall thickness and spacing between the two regular arrays of pore channel of mesoporous silica supports calculated from the SAXRD and N_2 absorption–desorption isotherms.

Samples	$d_{(100)}$ (nm)	a_o (nm)	Pore wall thickness (nm)
MCM-41	4.03	4.65	1.25
FSM-16	3.38	3.91	1.40
SBA-15	8.40	9.70	3.55

the micropores are completely blocked by the Co-B as indicated by the disappearance of the hysteresis loop. Nevertheless, from the above nitrogen adsorption results it is very difficult to visualize the location of the Co-B particles whether they lie inside the channels of pores or they are covering the pores from external surface. Thus, for better understanding, TEM was carried out for all the samples.

Unsupported Co-B powder is mainly composed of spherical particles with size in the range of 30–40 nm (SEM image in Fig. 3a of ref [37]). However, due to the exothermic nature of the reduction reaction and the high surface energy involved, these particles are mostly present in agglomerated state to acquire low specific surface area. In addition, ferromagnetic nature of the Co-B particles can also assist in agglomeration of NPs. TEM images show that NPS particles prepared by Stober method are perfectly spherical with narrow size distribution in the range of 150–160 nm (Fig. 4a). Co-B particles supported on these NPS showed similar size (30–40 nm) and morphology to that of unsupported Co-B catalyst with slightly less agglomeration (Fig. 4b).

MCM-41 silica particles mainly acquire irregular spherical shape with size in the range of 80–120 nm (Fig. 4c). The surface of these particles is composed of regular hexagonal arrays of mesopores with uniform pore size as shown in the TEM image of MCM-41 (Inset of Fig. 4c). The distance that is repeated between the pores is measured around 4.5 nm, which is in perfect agreement with the spacing value (a_o) (Table 2) obtained from the peak in the SAXRD pattern. The pore size and wall thickness were measured around 3.2–3.5 nm and 1–1.3 nm, respectively. These values are consistent to those obtained by SAXRD and BET measurement (Table 2). Crumpled paper like structure was observed for FSM-16 silica (Fig. 4e). TEM viewed down in the direction of the pore axis reveals a hexagonally ordered mesoporous structure with regular arrangement of pores of uniform size. The pores are seen to be arranged in the patches composed of regular rows on the silica sheet with the spacing of 4 nm between them. This value along with pore size (2.3–2.5 nm) and pore wall (1.2–1.4 nm) measured by TEM is in good agreement with that obtained by the structural and N_2 adsorption data (Tables 1 and 2). Like FSM-16 and MCM-41, SBA-15 type silica also shows well ordered hexagonal arrays of 2D mesoporous channels, especially along the direction of the pore axis (Fig. 4g) or in the direction perpendicular to the pore axis (Fig. 4i). However, the pores here are well distinct with bigger size (6.2 nm) and walls are much thicker (3.5 nm) than the other two mesoporous materials. Even though all the three mesoporous silica have the similar pore structures, they accommodate Co-B particles in a quite different manner. As observed by the TEM micrograph, the Co-B particles are located on the outer surface of MCM-41 (Fig. 4d) and FSM-16 (Fig. 4f) silica while the catalyst particles are well placed inside the channel of the SBA-15 type silica (Fig. 4h and j). This was concluded on the basis that the porous structure of FSM-16 and MCM-41 is not visible while for SBA-15, the hexagonal array structure is well maintained after Co-B loading. The Co-B particles are well confined in the pores of SBA-15 acquiring the size of pores (~6 nm) (Fig. 4h). Along the channel, the size of Co-B slightly increases to around 10 nm (Fig. 4j). In case of FSM-16 and MCM-41, the Co-B particles are well dispersed on the surface having broad distribution of size in the range from 3 to 30 nm. However, most of them (90%) have size lower than 15 nm. Due to the irregular shape of particles and large thickness of the support, the determination of the exact particle size is hindered. Roughly calculated average particle size is about ~10 nm and ~12 nm for MCM-41 and FSM-16, respectively. Particle size greater than the pore size confirms that Co-B particles are located on the surface of the MCM-41 and FSM-16 type silica with some portion of the particle anchored into the pores. SAED pattern for Co-B particles supported on all three mesoporous silica exhibits diffuse diffraction rings thereby confirming

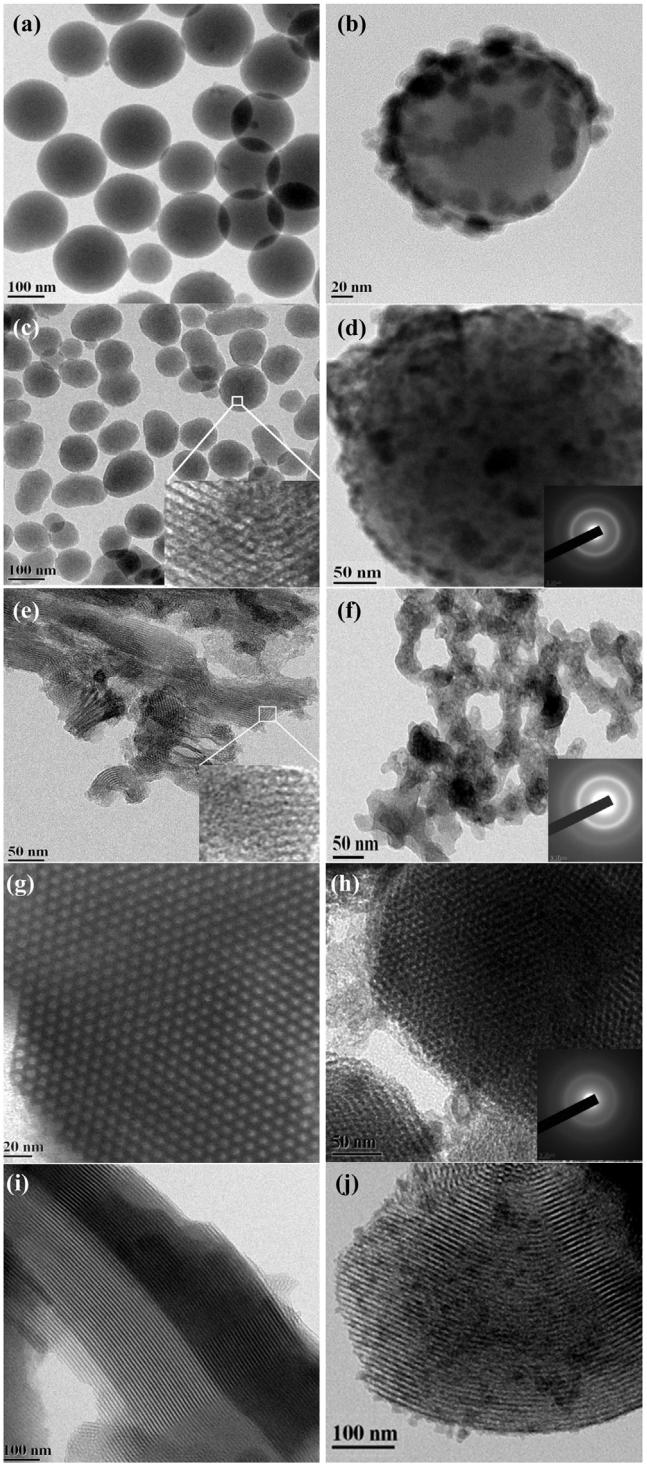

Fig. 4. Bright field TEM micrograph of bare (a) NPS, (c) MCM-41, (e) FSM-16, (g) and (i) SBA-15 type silica supports while (b), (d), (f), (h) and (j) shows micrographs of corresponding supports with Co-B catalyst loading.

the amorphous nature of Co-B particle as observed in the XRD pattern. The morphological analysis clearly shows that the particles do not directly acquire the size of the support pores and depending on the texture of the mesopores, the particles are located on the pores. The different morphologies obtained on different mesoporous silica are attributed to the impregnation–reduction process. During impregnation, $CoCl_2$ solution fills most of the pores of mesoporous silica by capillary action. Generally, during the reduction process

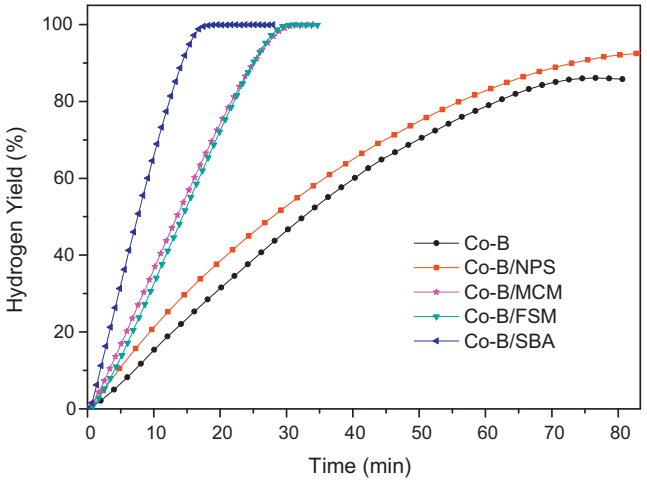

Fig. 5. Hydrogen generation yield, as a function of reaction time, obtained by hydrolysis of AB (0.025 M) in the presence of unsupported Co-B catalyst powder, and that supported over NPS, MCM-41, FSM-16, and SBA-15 type silica supports.

by $NaBH_4$, the Co-B particles are formed by release of H_2 gas. Thus, in case of SBA-15, due to the interconnected pore assembly H_2 can leave the interior of the SBA-15 easily. In FSM-16 and MCM-41, the pores are not connected and thus, in this case, H_2 can be released only from the pore face which is blocked by the Co-B particles. Thus, due to the pressure exerted by the H_2 gas, the Co-B particles are pushed out on the external surface of MCM-41 and FSM-16. The other possibility is that due to the limitation of the preparation method, Co-B particle size cannot be reduced lower than the size of mesopores of MCM-41 and FSM-16 to accommodate it. However, the average size of Co-B particles is around 10–12 nm for MCM-41 and FSM-16 silica with a size distribution from 3 to 30 nm. This is attributed to the fact that $CoCl_2$ not only fills the pores but is also additionally adsorbed on the surface of the support. Thus, when $CoCl_2$ in the pores is reduced by $NaBH_4$ solution, it forms Co-B particles which act as nucleation site for Co-B particles formed on the support surface to grow further. Since large numbers of nucleation sites are available in the form of regularly arranged pores, most of the particles do not grow larger than 10–12 nm. However, some of the pore channels on the surface are not impregnated with $CoCl_2$ solution; thus, Co-B particles formed around these pores may agglomerate to form big particles having size of about 30 nm on the outer surface similar to the case of NPS. High degree of dispersion of these nanoparticles is obtained due to the presence of large number of nucleation sites in the form of mesopores in MCM-41 and FSM-16.

The catalytic activity of Co-B particles supported over various silica (non-porous and mesoporous) was tested for H_2 production by hydrolysis of AB. H_2 generation yield was measured, as a function of time, during the hydrolysis of AB solution (0.025 M) in the presence of Co-B catalyst loaded onto NPS, MCM-41, FSM-16 and SBA-15 type silica and Co-B unsupported powder at 298 K (Fig. 5). The amount of Co-B (10 mg) loading was kept same for all the catalyst powders. The catalyst weight was thus selected to maintain $NaBH_4$ to catalyst molar ratio around 50. Active nature of all the catalyst powders was confirmed by the fact that H_2 is instantaneously produced as soon as they come in contact with the AB solution. Irrespective of type, Co-B supported on mesoporous silica definitely shows higher catalytic activity as compared to Co-B supported on NPS (73 min) and unsupported Co-B catalyst (75 min), and has the ability to complete the reaction within considerably less time (15 min). Among all the mesoporous materials, Co-B supported on the SBA-15 type silica (15 min) was the fastest to complete the reaction: the time taken was two times lesser than that observed for MCM-41 (29 min) and FSM-16 (30 min) supported Co-B catalyst. Expected amount of H_2 ($H_2/NH_3BH_3 = 3$) was produced by Co-B when supported on mesoporous silica of different types, while only 85% of H_2 is produced by unsupported Co-B and that supported on NPS. Negligible activity for H_2 generation is obtained by using the bare mesoporous and non-porous silica supports without Co-B loading. The H_2 generation yield values reported in Fig. 5 was perfectly fitted by single exponential function for unsupported and NPS supported Co-B catalyst powders. This indicates that hydrolysis reaction proceeds following the first order kinetics with respect to AB concentration. On the contrary, linear function was required to fit the H_2 production data for Co-B supported on all the mesoporous silica materials thus proving zero order kinetic reaction with respect to AB concentration. The maximum H_2 generation rate (R_{max}) achieved by Co-B supported on SBA-15 silica (~1900 ml/min/g of Co-B catalyst) is 4.2 and 5.3 times higher than that obtained by NPS supported Co-B (~480 ml/min/g of Co-B catalyst) and unsupported Co-B powder catalyst (~360 ml/min/g of Co-B catalyst). For mesoporous silica supports, Co-B supported on SBA-15 showed highest H_2 generation rate which is about 1.5 times higher than that measured with MCM-41 (~1150 ml/min/g of Co-B catalyst) and FSM-16 (~1200 ml/min/g of Co-B catalyst). The obtained H_2 generation rate value with SBA-15 supported Co-B catalyst is definitely better than that of Co-B nanospindles (1293 ml/min/g of catalyst) [38], and amorphous Co-B catalyst used under ultrasonic hydrolysis reaction (395 ml/min/g of catalyst) [39], and comparable to transition metal doped Co-B [11]. Co-B thin film catalyst synthesized by pulsed laser deposition shows better H_2 generation rate than presently obtained, but the laser deposition process permits to synthesize catalyst having unique nanostructure of Co NPs (10 nm) embedded in boron matrix [7,8].

The catalytic performance of Co-B catalyst supported on NPS is almost similar to that of unsupported Co-B catalyst, a result that may be mainly attributed to the similar morphological characteristic observed in both the cases. Higher activity of Co-B supported on mesoporous silica is ascribed to the presence of smaller size (6–12 nm) Co-B particles with proper dispersion on the surface. This scenario provides large number of under-coordinated Co active atoms for the interaction with reactant to produce expected amount of H_2 with much higher rate than that of unsupported and NPS supported Co-B catalyst. By anchoring Co-B particles over the mesopores could avoid agglomeration thus ensuring high effective surface area during the course of catalysis reaction. This is the main reason for the observed zero order reaction with respect to AB concentration for mesoporous silica supported Co-B catalyst. For mesoporous silica, SBA-15 showed the best catalytic activity which is mainly attributed to the Co-B particle confinement in the mesopores. Due to the confinement, Co-B particles acquires the size of the pores (~6 nm) which is smaller than the size of Co-B particles supported over MCM-41 (~10 nm) and FSM-16 (~12 nm) silica. As observed from the TEM image, the pore size of SBA-15 is highly uniform. Thus, the Co-B particles also acquire a very narrow size distribution, unlike MCM-41 and FSM-16 supported Co-B particles having size distribution in the range of 3–30 nm. The pores in SBA-15 are open from both ends with internal interconnectivity to provide easy passage for reactant and product solutions as well as for the produced H_2 gas. Confinement of Co-B particle in the pores also eliminates any possibility of agglomeration during the reaction course and high temperature treatments. This shows that not only the size of the pores but also its texturing affects the location, size and dispersion of the Co-B catalyst particle. The H_2 production rate obtained with the catalyst supported over MCM-41 and FSM-16 is same, mostly due to the similar size (~10 to 12 nm) and location of the Co-B particles on support surface anchored with the pores.

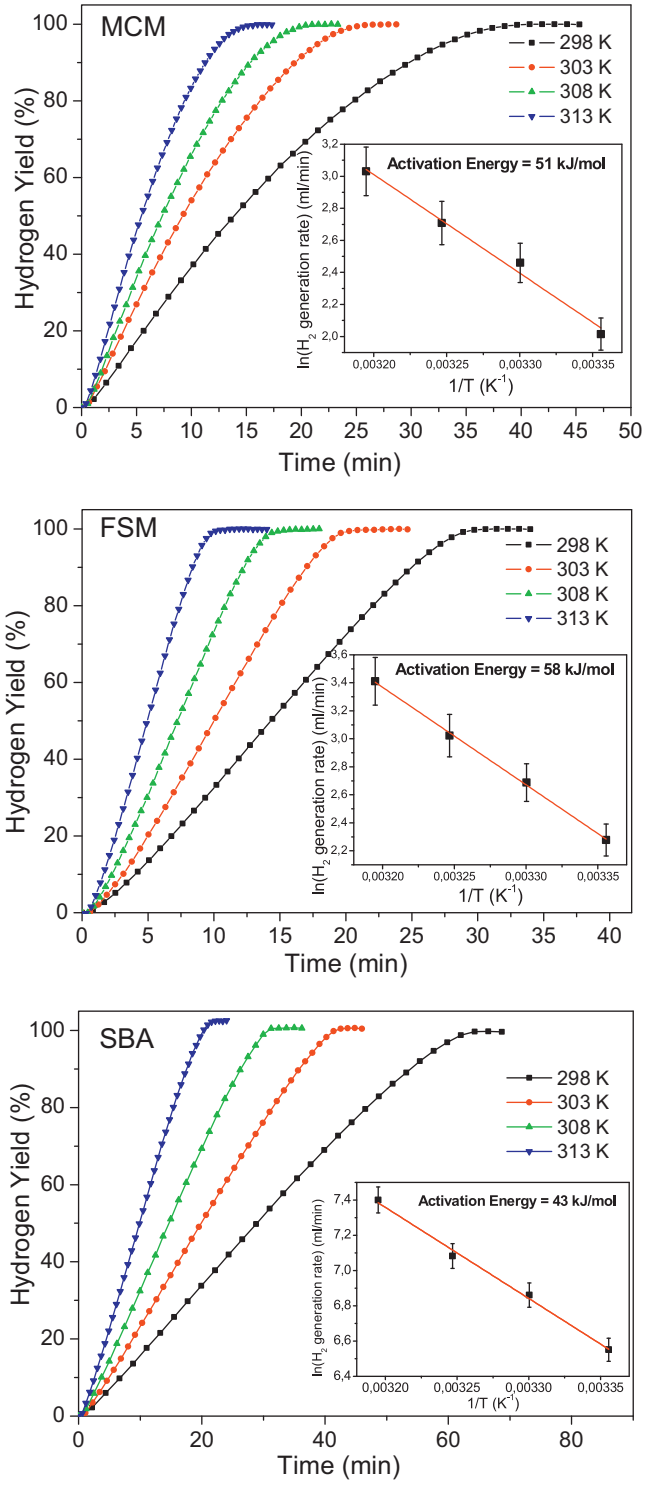

Fig. 6. Hydrogen generation yield, as a function of reaction time, obtained by hydrolysis of AB (0.025 M) at 4 different solution temperatures in the presence of MCM-41, FSM-16, and SBA-15 type silica supported Co-B catalyst. Inset shows the Arrhenius plot of the H_2 generation rates for each support.

In order to confirm the effectiveness of Co-B catalyst supported on SBA-15, activation energy barrier was evaluated by varying AB solution temperature. The H_2 generation yield, as a function of time, was measured at different solution temperatures by hydrolysis of AB (0.025 M) solution using Co-B catalyst supported over MCM-41, FSM-16 and SBA-15 type mesoporous silica as reported in Fig. 6. The evaluation of activation energies of rate limiting step is carried out

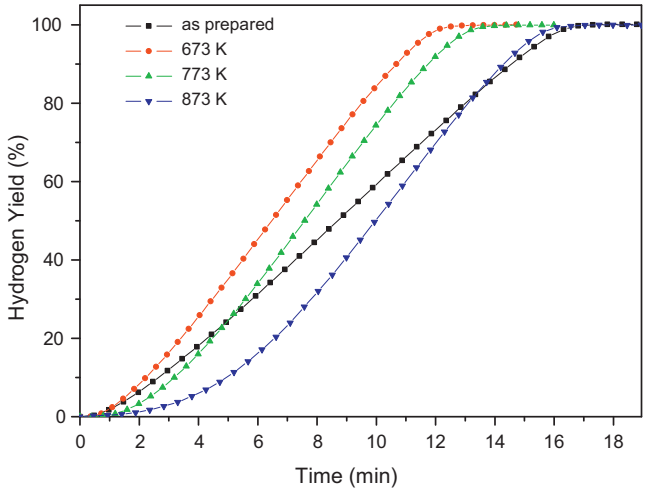

Fig. 7. Hydrogen generation yield, as a function of reaction time, obtained by hydrolysis of AB (0.025 M) in the presence of untreated Co-B catalyst supported over SBA-15 type silica and that heat treated in Ar atmosphere for 2 h at 673, 773, and 873 K.

from Arrhenius plot (inset of Fig. 6) of the H_2 generation rate. Co-B catalyst supported on SBA-15 (43 ± 2 kJ/mol) displays significantly lower energy barrier value in comparison to Co-B supported on MCM-41 (51 ± 3 kJ/mol) and FSM-16 (58 ± 3 kJ/mol). The favorable activation energy again provides an evidence that confinement of Co-B particles in the pores with interconnectivity is well suited for the catalytic hydrolysis reaction. In general, the obtained activation energies are lower than that obtained with Rh (67 kJ mol^{-1}) nanoclusters [40], Ru/C (76 kJ mol^{-1}) [5], K_2PtCl_6 (86 kJ mol^{-1}) [3], NiAg (51.5 kJ mol^{-1}) [41], Co/α-Al_2O_3 (62 kJ mol^{-1}) [42], and comparable to Pd metal (44 kJ mol^{-1}) [6], Co-Mo-B/Ni foam (44 kJ mol^{-1}) [43], Ru (47 kJ mol^{-1}) [4], and Co (0) nanoclusters (46 kJ mol^{-1}) [44].

Generally, unsupported Co-B particles agglomerate when heated at elevated temperatures in anaerobic conditions to form big crystallites [45]. This agglomeration initiates above the treatment temperature of 473 K and the related kinetics reach maximum at 773 K to form micron sized crystals of metallic Co [46]. This modification strongly hinders the catalytic activity of the Co-B catalyst. The heat treatment at 873 K completely deteriorates the catalytic efficiency of the Co-B catalyst [12]. The stability of Co-B particles confined in the pores and robustness of the pore structure was tested by heat treating the Co-B catalyst supported over SBA-15 silica at elevated temperatures (673, 773, and 873 K) in Ar atmosphere for 2 hours. The H_2 generation yield, as a function of time, obtained by hydrolysis of AB (0.025 M) solution using these heat treated Co-B supported over SBA-15 silica catalysts are reported in Fig. 7. H_2 generation rate increases when SBA-15 supported catalyst was treated at 673 K and just 10 minutes are required to complete the reaction. However, further increase in treatment temperature to 773 K causes slight decrement in the catalytic activity but it is still higher than the untreated catalyst. At 873 K, the initial induction time was increased slightly to 2 min but later, during the reaction course, the H_2 generation rate increases and the reaction is completed in same time as that of untreated sample. This result indicates that, while unsupported Co-B particles get completely deteriorated by heat treating at 873 K, when confined in the pores of SBA-15 they maintain their catalytic activity similar to that of untreated catalyst. Unsupported amorphous Co-B powder undergoes crystallization when heated above 473 K in anaerobic condition to form Co_2B phase which is very active phase for hydrolysis of chemical hydrides [43]. But above 673 K the agglomeration of Co-B particles increases to form big clusters which decompose to

form metallic Co crystallites of micron size. This process, especially the decomposition of Co-B to Co metal crystallite, mainly due to the high degree of agglomeration, strongly decreases the catalytic activity of the Co-B alloy catalyst. For SBA-15 supported Co-B, the particles lie within the pores where Co_2B active phase is formed in the temperature range of 473–673 K which is responsible for the improvement of the catalytic performance of the supported catalyst at elevated temperatures (673 and 773 K). At higher temperatures the confinement of Co-B particles in the pores possibly avoids the agglomeration of the neighboring particles thus hindering the decomposition of Co_2B phase to form inactive metallic Co phase. Thus, even at 873 K, high H_2 generation rate is maintained with slight induction time (2 min).

4. Conclusions

The H_2 production by hydrolysis of AB was studied by using Co-B NPs catalyst supported by impregnation–reduction method over three kinds of mesoporous silica (MCM-41, FSM-16, and SBA-15) of different pore size and texture. TEM images and N_2 adsorption–desorption isotherm revealed that size, dispersion degree, and location of Co-B NPs are affected by the pore texturing of the support. Co-B supported over SBA-15 silica was found to be most active catalyst that produces the expected amount of H_2 gas from hydrolysis of AB with H_2 generation rate of about 1900 ml/min/g of Co-B catalyst, a value that is definitely higher than that measured with MCM-41 (∼1150 ml/min/g of Co-B catalyst) and FSM-16 (∼1200 ml/min/g of Co-B catalyst).

The higher efficiency of Co-B supported on SBA-15 is explained on the basis of the geometrical confinement of Co-B particles within the pores with Co-B NPs that have average size of about 6 nm and uniform size distribution while exhibiting higher degree of dispersion. The effective activation energy of the rate limiting process in hydrolysis operated by Co-B NPs with interconnected pores of SBA-15 results lower than that established with MCM-41 and FSM-16 supported catalyst. Finally, the thicker pore walls of SBA-15 support avoids agglomeration of the Co-B NPs thus providing high stability at elevated temperatures (873 K) as opposed to what occurs with unsupported Co-B NPs catalyst.

Acknowledgements

We thank S.N. Achary and M. Thigle for XRD analysis, and P. Kadam for BET measurements. The research activity is partially supported by “Fondazione Cassa di Risparmio di Trento e Rovereto”.

References

[1] U.B. Demirci, P. Miele, Energy & Environmental Science 2 (2009) 627–637.
[2] F.H. Stephens, V. Pons, R.T. Baker, Dalton Transactions 25 (2007) 2613–2626.
[3] N. Mohajeri, A.T. Raissi, O. Adebiyi, Journal of Power Sources 167 (2007) 482–485.
[4] F. Durap, M. Zahmakiran, S. Ozkar, International Journal of Hydrogen Energy 34 (2009) 7223–7230.
[5] V.I. Simagina, P.A. Storozhenko, O.V. Netskina, O.V. Komova, G.V. Odegova, Y.V. Larichev, A.V. Ishchenko, A.M. Ozerova, Catalysis Today 138 (2008) 253–259.
[6] O. Metin, S. Sahin, S. Ozkar, International Journal of Hydrogen Energy 34 (2009) 6304–6313.
[7] N. Patel, R. Fernandes, G. Guella, A. Miotello, Applied Catalysis B: Environmental 95 (2010) 137–143.
[8] N. Patel, A. Miotello, V. Bello, Applied Catalysis B: Environmental 103 (2011) 31–38.
[9] A. Baiker, Faraday Discussions of the Chemical Society 87 (1989) 239–251.
[10] Z. Wu, S. Ge, Catalysis Communications 13 (2011) 40–43.
[11] R. Fernandes, N. Patel, A. Miotello, R. Jaiswal, D.C. Kothari, International Journal of Hydrogen Energy 37 (2012) 2397–2406.
[12] R. Fernandes, N. Patel, A. Miotello, R. Jaiswal, D.C. Kothari, International Journal of Hydrogen Energy 36 (2011) 13379–13391.
[13] N. Patel, R. Fernandes, A. Miotello, Journal of Catalysis 271 (2010) 315–324.
[14] D. Tong, W. Chu, Y.Y. Luo, H. Chen, X.Y. Ji, Journal of Molecular Catalysis A: Chemical 269 (2007) 149–157.
[15] N. Patel, R. Fernandes, N. Bazzanella, A. Miotello, Catalysis Today 170 (2011) 20–26.
[16] N. Patel, R. Fernandes, A. Santini, A. Miotello, International Journal of Hydrogen Energy 37 (2012) 2007–2013.
[17] I. Yuranov, P. Moeckli, E. Suvorova, P. Buffat, L. Kiwi-Minsker, A. Renken, Journal of Molecular Catalysis A: Chemical 192 (2003) 239–251.
[18] J.S. Beck, J.C. Vartuli, W.J. Roth, M.E. Leonowicz, C.T. Kresge, K.D. Schmitt, C.T. Chu, D.H. Olsen, E.W. Sheppard, S.B. McCullen, J.B. Higgins, J.L. Schlenker, Journal of the American Chemical Society 114 (1992) 10834–10843.
[19] Q. Huo, D.I. Margolese, U. Ciesla, D.G. Demuth, P. Feng, T.E. Gier, P. Sieger, A. Firouzi, B.F. Chemelka, F. Schüth, G.D. Stucky, Chemistry of Materials 6 (1994) 1176–1191.
[20] V. Kocherbitov, V. Alfredsson, Langmuir 27 (2011) 3889–3897.
[21] K. Moller, T. Bein, Chemistry of Materials 10 (1998) 2950–2963.
[22] G.S. Attard, S.A.A. Leclerc, S. Maniguet, A.E. Russell, I. Nandhakumar, P.N. Bartlett, Chemistry of Materials 13 (2001) 1444–1446.
[23] H.Z. Shi, L.D. Zhang, W.P. Cai, Materials Research Bulletin 35 (2000) 1689.
[24] Y.J. Han, J.M. Kim, G.D. Stucky, Chemistry of Materials 12 (2000) 2068–2069.
[25] X. Chen, S. Wang, J. Zhuang, M. Qiao, K. Fan, H. He, Journal of Catalysis 227 (2004) 419–427.
[26] H. Li, J. Liu, H. Yang, H. Li, Chinese Journal of Chemistry 27 (2009) 2316–2322.
[27] C.Y. Lai, B.G. Trewyn, D.M. Jeftinija, K. Jeftinija, S. Xu, S. Jeftinija, S.Y. Victor Lin, Journal of the American Chemical Society 125 (2003) 4451–4459.
[28] A. Matsumoto, T. Sasaki, N. Nishimiya, K. Tsutsumi, Colloids and Surfaces A: Physicochemical and Engineering Aspects 203 (2002) 185–193.
[29] V. Brahmkhatri, A. Patel, Applied Catalysis A-General 403 (2011) 161–172.
[30] W. Stober, A. Fink, E. Bohn, Journal of Colloid and Interface Science 26 (1968) 62–69.
[31] C. Zanchetta, B. Patton, G. Guella, A. Miotello, Measurement Science and Technology 18 (2007) N21–N26.
[32] D. Zhao, J. Feng, Q. Huo, N. Melosh, G.H. Fredrickson, B.F. Chmelka, G.D. Stucky, Science 279 (1998) 548–552.
[33] M.S. Ghattas, Microporous and Mesoporous Materials 97 (2006) 107–113.
[34] K.S.W. Sing, D.H. Everett, R.A.W. Haul, L. Moscou, R.A. Pierotti, J. Rouquerol, T. Siemieniewska, Pure and Applied Chemistry 57 (1985) 603.
[35] D. Zhao, Q. Huo, J. Feng, B.F. Chmelka, G.D. Stucky, Journal of the American Chemical Society 120 (1998) 6024–6036.
[36] Y. Luo, Z. Hou, R. Li, X. Zheng, Microporous and Mesoporous Materials 109 (2008) 585–590.
[37] N. Patel, R. Fernandes, R. Edla, P.B. Lihitkar, D.C. Kothari, A. Miotello, Catalysis Communications 23 (2012) 39–42.
[38] D.G. Tong, X.L. Zeng, W. Chu, D. Wang, P. Wu, Journal of Materials Science 45 (2010) 2862–2867.
[39] A.K. Figen, B. Coskuner, International Journal of Hydrogen Energy 33 (2008) 2462–2467.
[40] H. Li, W. Wang, H. Li, J.F. Deng, Journal of Catalysis 194 (2000) 211–221.
[41] N. Patel, R. Fernandes, G. Guella, A. Kale, A. Miotello, B. Patton, C. Zanchetta, Journal of Physical Chemistry C 112 (2008) 6968–6976.
[42] M. Zahmakiran, S. Ozkar, Applied Catalysis B: Environmental 89 (2009) 104–110.
[43] C.F. Yao, L. Zhuang, Y.L. Cao, X.P. Ai, H.X. Yang, International Journal of Hydrogen Energy 33 (2008) 2462–2467.
[44] Q. Xu, M. Chandra, Journal of Power Sources 163 (2006) 364–370.
[45] H. Li, H. Yang, H. Li, Journal of Catalysis 251 (2007) 233–238.
[46] H. Li, X. Chen, M. Wang, Y. Xu, Applied Catalysis A-General 225 (2002) 117–130.